Sialoglycans Modulate Siglec-5 – TLR4 Interactions in Osteoarthritis

Authors: Loise Råberg[1], Fan Jia[1], Ula von Mentzer[1], Vignesh Venkatakrishnan[1], Niclas G. Karlsson[2], Alexandra Stubelius[1*]

Affiliations:
[1] Division of Chemical Biology, Department of Life Sciences, Chalmers University of Technology, Gothenburg, SE-412 96, Sweden.
[2] Department of Life Sciences and Health, Faculty of Health Sciences, Oslo Metropolitan University Oslo Metropolitan University, Oslo, Norway

[*]**Corresponding author:**
Alexandra Stubelius (alexandra.stubelius@chalmers.se)
Chalmers University of Technology
Department of Life Sciences
Division of Chemical Biology
Kemigården 4
SE-412 96 Göteborg,
Sweden
+46(0)31-772 4101

Keywords: Osteoarthritis, Monocytes, Siglec-5, Sialic Acid, TLR4

Summary:
Osteoarthritis (OA) is characterized by chronic, low-grade inflammation that contributes to cartilage degradation and joint pain. We previously identified Siglec-5 in synovial fluid of OA patients (OA SF), which prompted us to investigate its interaction with the sialylated proinflammatory receptor TLR4 in monocytes. Here, we reveal an inverse correlation between Siglec-5 and TLR4, suggesting Siglec-5 may suppress inflammation. To gain mechanistic insights, monocytes stimulated with OA SFs were compared to M-CSF, LPS, and sialidase, to assess patient-specific inflammatory pathways and phenotypes. Notably, OA SF that triggered elevated IL-6 production in monocytes exhibited phenotypes similar to those of LPS- or sialidase-treated cells, reinforcing the role of sialylation patterns influencing OA severity. To confirm direct interaction of Siglec-5 and TLR4, colocalization was analyzed, displaying a time- and sialoglycan- dependent interaction. These findings reveal a Siglec-5-TLR4 axis modulated by sialylation, highlighting a potential strategy for mitigating inflammation and preserve joint integrity in OA.

INTRODUCTION

Osteoarthritis (OA) is the most common degenerative joint disorder worldwide, characterized by synovitis, cartilage degradation and subchondral bone remodeling that severely impacts quality of life. [1] This complex condition involving mechanical stress and inflammatory pathways displays significant variability between patients. Persistent inflammation stem from both tissue-resident and infiltrating immune cells, including monocytes, which play key roles in perpetuating inflammation. [2,3] Upon recruitment, monocytes are polarized into a pro-inflammatory phenotype in response to the local environment, contributing to the cycle of tissue damage and degeneration of cartilage. [4,5] The multifactorial nature of OA coupled to the limited regenerative capacity of cartilage has posed a major challenge both for finding relevant biomarkers and developing effective treatments. Despite extensive efforts, clinical trials targeting cytokines such as IL1β and TNFα have not yielded significant therapeutic benefits, underscoring the need for alternative mechanistic insights and novel intervention strategies. [6-8]

Recent advances in nanotherapeutics have offered promising new approaches, as they can deliver drugs to the deeply embedded cells in the cartilage responsible for OA progression. [9] In our previous work, we explored the interactions between a family of small dendritic polyamidoamine (PAMAM)-based nanoparticles (NPs) and synovial fluid (SF) proteins from OA patients. [10] By proteomics, we identified a high abundance of Sialic acid-binding immunoglobulin-like lectin-5 (Siglec-5) in the proteins associated with the NPs, suggesting a potential involvement in OA pathogenesis. Siglecs are gaining increasing attention in multiple diseases, including cancer, sepsis, and autoimmune disorders due to their immunomodulatory functions and potential for therapeutic targeting. [11-13] Siglec-5 has been found in sepsis, Siglec-9 in arthritis, and Siglec-15 plays an important role in macrophage fusion into osteoclasts but so far, the role of Siglec-5 has not been reported in OA. [14-16] Through their affinity to sialic acid (Sia), Siglecs act as key regulators of monocyte activation, recruiting the tyrosine SHP-1 and SHP-2, to counterbalance pro-inflammatory pathways. [17] Siglec-5 is mostly found on cell surfaces on monocytes, macrophages, and T cells. However, soluble Siglec-5 has been identified and was shown to inhibit $CD8^+$ T cell proliferation in sepsis, and soluble Siglec-9 demonstrated immunosuppressive effects on macrophages in arthritis models. [14,16,18]

In arthritis, upregulated Siglec-9 has been identified and murine Siglec-E, the mouse ortholog of human Siglec-9 has been shown to regulate pattern recognition receptors (PRRs). [14,19] PRRs, such as toll-like receptor 4 (TLR4), play a key role in OA, its activation can be induced by structural fragments of damaged cartilage. [20,21] TLR4 recognizes solubilized fragments of glycoproteins such as collagen type-II, hyaluronan, aggrecan, and lubricin which are present in OA SF and function as damage-associated molecular patterns (DAMPs), thereby exacerbating joint inflammation. [22-24] TLR4 is gaining increasing interest as its activation disrupts immune homeostasis and contributes to the onset and progression of age-related diseases, including OA. [25] Through the NF-κB pathway pro-inflammatory cytokines such as IL-1, IL-6, IL-8, and tumor necrosis factor (TNFα) are released in the joint, aggravating joint degradation and OA symptoms, however it's regulation is poorly understood in OA. [3,21,26-29]

TLR4 activity is influenced by its internalization dynamics and glycosylation decorations. Specifically, its sialylation patterns play a pivotal role in modulating TLR4 signaling. [19,30,31] In general, endogenous activity of sialyltransferases and sialidases are regulated upon monocyte activation and differentiation, and alteration in sialyltransferase expression have been identified in OA cartilage. [32-34] It has been shown that LPS can trigger sialidase relocation to the cell surface, where it desialylates TLR4 and promotes its activation. [35] Interestingly, Siglec-E counteracts this process by binding Sia residues on TLR4, leading to either internalization or shedding of TLR4 to reduce inflammation. [19,36-38] Both Siglec-9 and Siglec-5 have shown high affinity to TLR4, indicating their immunomodulatory role of TLR4 signaling.[30] Siglec-5 has however not been studied as extensively as Siglec-9, which could be due to lack of a mouse ortholog. [16,17] As we had identified Siglec-5 in the SF of OA patients, the purpose of this study was to investigate the regulatory relationship between Siglec-5, Siglec-9, Siglec-15 and TLR4 in monocyte stimulated with OA SF.

We found an inverse correlation between membrane-associated Siglec-5 and TLR4 expression by flow cytometric profiling, suggesting that engaging Siglec-5 dampens excessive inflammatory responses. To gain mechanistic understanding we employed stimulations including macrophage-colony stimulating factor (M-CSF), IL1β/TNFα, LPS, and sialidase to understand patient-specific inflammatory pathways and phenotypes. Further insights of crosstalk between Siglec-5 with TLR4 and Siglec-9, was gained through inhibition of TLR4 signaling using the small molecule inhibitor TAK-242. Our findings suggest that Siglec-5 can serve as a modulator of TLR4-driven low-grade inflammation. High-grade inflammatory conditions induced by LPS or Sialidase displayed similar cytokine profiles both with and without TAK-242, indicating that sialoglycans are critical regulators of TLR4-driven inflammation. Overall, our findings suggest that Siglec-5, but not Siglec-9 and Siglec-15, through Sia expression on cells could present an endogenous regulatory pathway to fine tune and mitigate inflammation to reduce cartilage degradation in OA.

RESULTS

Siglec-5 can be found in synovial fluid from osteoarthritis patients and membrane-associated Siglec-5 negatively correlates with TLR4 expression on monocytes

NPs can be used as enrichment tools to identify proteins associated with pathogenic regulation. In a previous study, we developed a set of NPs which were incubated with OA SF where the proteins were identified through proteomics.[10] Amongst the proteins found in association with the NPs we identified Siglec-5 as one of the 14 most abundant entities (Figure 1A). As Siglec-5 functions as an inhibitory receptor, we used the IntAct database to find a potential regulated partner and discovered a medium relationship (MI score 0.54) between TLR4 and Siglec-5 (Figure 1B), suggesting an unexplored regulatory pathway in OA.[39] Interestingly, both of these receptors can be found on monocytes, which is the most abundant immune cells in the OA joint .[40]

Monocyte function can be classified into different subsets based on their expression of CD14 and CD16.[41,42] The intermediate $CD14^{+}CD16^{+}$ subset presents antigens and secretes cytokines and has been found in greater abundance in the joint of OA patients.[40] In this study, we isolated blood-derived monocytes and confirmed their relative percentage of subsets (Figure S1, Figure S2A and S2B). Figure 1C shows the gating strategy at baseline, where all monocytes were positive for Siglec-5^{+} (purple) and Siglec-9 (not shown), whereas the percentage $TLR4^{+}$ monocytes were mainly found in the classical and intermediate population (green). We found that monocytes cocultured with OA SFs for 24hrs generated an intermediate monocyte population consisting of more than 50% of the population (Figure 1D and 1E). Compared to baseline, the classical monocytes decreased, and non-classical monocytes were completely absent. While most cells remained positive for Siglec-5 (purple), TLR4 (green) expression was reduced.

The monocyte subsets were further analyzed for their baseline expression of TLR4, Siglec-5, Siglec-9, and Siglec-15. Classical monocytes displayed the highest expression of TLR4, Siglec-5, and Siglec-9, whereas Siglec-15 was not detected on any subset (Figure S2C-E and Figure S3). After 24h of OA SF stimulations, multiple OA SFs led to a significant upregulation in Siglec-5 expression on monocytes (Figure 1G). In contrast to previous murine studies, Siglec-9 was only upregulated in one patient (Figure 1H). Correlation analysis confirmed an inverse relationship between Siglec-5 with TLR4 and intermediate monocytes (Figure 1I and 1J), whereas no correlation was observed between Siglec-9 with TLR4 and intermediate monocytes (Figure 1K and 1L). A correlation between Siglec-5 to Siglec-9, and intermediate monocytes to TLR4 could not be established (Figure S4A and S4B).

In summary, the monocytes shifted toward the intermediate subset after SF stimulation. Correlation analysis revealed an inverse relationship between Siglec-5, TLR4, and intermediate monocytes, but not with Siglec-9, suggesting interactions specifically between TLR4 and Siglec-5 in OA.

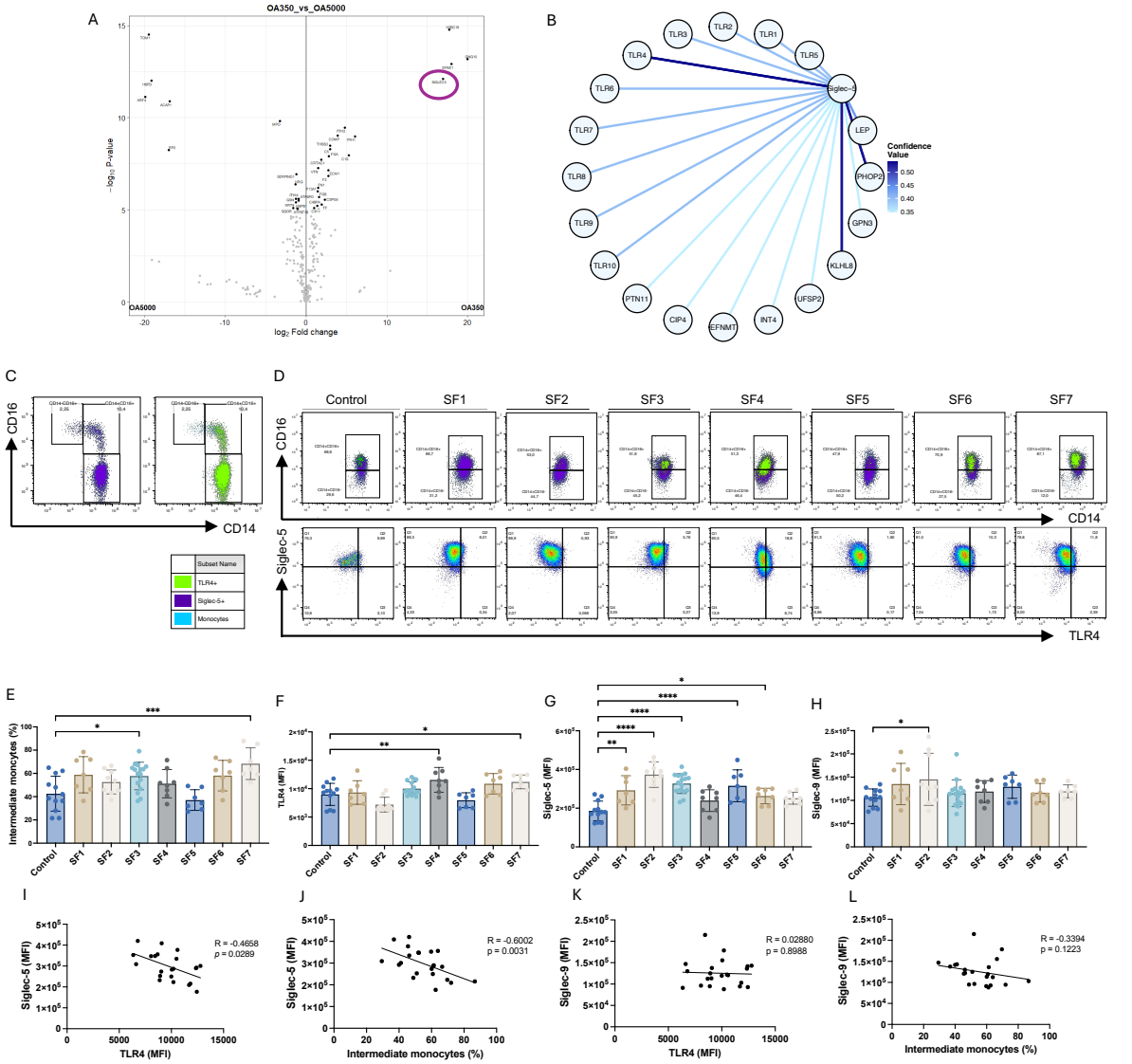

Figure 1. Siglec-5 can be found in synovial fluid from osteoarthritis patients and membrane-associated Siglec-5 negatively correlates with TLR4 expression on monocytes

(A) Volcano plot displaying the proteins detected in the protein in association with $PAMAM_{5000}$ and $PAMAM_{350}$, here denoted OA5000 and OA350 using proteomics analysis. Siglec-5 is indicated with a circle.

(B) Protein-protein interaction network visualized from the IntAct database. Medium evidence of interaction appears to TLR4, PHOP2, and KLHL8, where TLR4 had the highest confidence value with a MI score of 0.54. The illustration was adopted from the website and resolution and color scheme improved using R.

(C) Representative flow cytometric dot plots displaying the baseline levels (0hrs) of classical, intermediate, and non-classical subsets, where blue color represents all monocytes, purple color represents Siglec-5^+, and green represents $TLR4^+$ cells.

(D) Representative flow cytometric dot plots of monocytes after 24hrs of coculture with OA SF. The plots display the ratio between classical and intermediate monocytes, where blue represents both subsets, purple represents Siglec-5^+ cells, and green represents $TLR4^+$ cells.

(E) Percentage intermediate monocytes ($CD14^+CD16^+$) after 24hrs of coculture with OA SF (n=3 from three biological replicates).

(F-H) Median fluorescence intensity (MFI) of TLR4, Siglec-5, and Siglec-9 on the cell membrane of monocytes after 24hrs of coculture with OA SF (n=3 from three biological replicates).

(I-L) Correlation between Siglec-5 to TLR4 and intermediate monocytes, and between Siglec-9 to TLR4 and intermediate monocytes (n=3 from three biological replicates).

Data is represented as mean±SD, statistical analysis was performed using one-way ANOVA with Dunnett's multiple comparisons test. Correlation analysis was performed using Spearman's correlation test (*p<0.05; **p<0.01; ***p<0.001; ****p<0.0001).

Siglec-5 regulate TLR4 signaling in inflammation

To investigate how specific signaling pathways dictate membrane expression of TLR4, Siglec-5, and Siglec-9, blood monocytes were isolated and subsequently stimulated with either M-CSF, IL1β/TNFα, or LPS. After 24hrs of stimulation with M-CSF and LPS, an expansion of intermediate monocytes where noted compared to baseline levels. The total monocyte population remained Siglec-5^+, while $TLR4^+$ monocytes decreased in the control and LPS (Figure 2A). We further assessed the expression dynamics of TLR4, Siglec-5, and Siglec-9 levels at 0, 4 and 24hrs of stimulation (Figure 2B-D). An initial increase in TLR4 could be observed already after 4hrs in the control and M-CSF, which remained after 24hrs. LPS reduced TLR4 expression already within 4 hours and this effect remained after 24hrs. Siglec-5 decreased across all groups after 4hrs of stimulation but recovered to basal level expression by M-CSF and LPS stimulations after 24hrs. All stimulations induced Siglec-9 expression after 4 and 24hrs compared to basal levels.

We proceeded with comparing the dynamics of the expression of intermediate monocytes, TLR4, Siglec-5, and Siglec-9 at 4 and 24hrs. For most stimulations, intermediate monocytes expanded continuously over 24hrs (Figure S5A, Figure 2E). TLR4 expression increased initially by M-CSF, while LPS reduced the expression of TLR4 compared to control at 4hrs (Figure S5B). After 24hrs, LPS continued to reduce TLR4 expression, whereas M-CSF and IL1β/TNFα produced comparable levels to control (Figure 2F, Figure S6A). Compared to the control, Siglec-5 and Siglec-9 expression remained the same across all stimulations at 4hrs (Figure S5C and S5D). After 24hrs of stimulation, M-CSF, IL1β/TNFα, and LPS had all induced a significant increase in Siglec-5 (Figure 2G, Figure S6B). In contrast, no significant alterations in Siglec-9 expression were observed by any stimulations at 24hrs (Figure 2H).

In summary, the intermediate monocyte population expanded over time, where TLR4 was reduced as Siglec-5 increased, displaying an interesting dynamic regulation pattern. This was true for both M-CSF and LPS, whereas IL1β/TNFα showed little regulation. Our data suggests complex interacting mechanisms governing TLR4 signaling, ultimately shaping the monocyte response in OA.

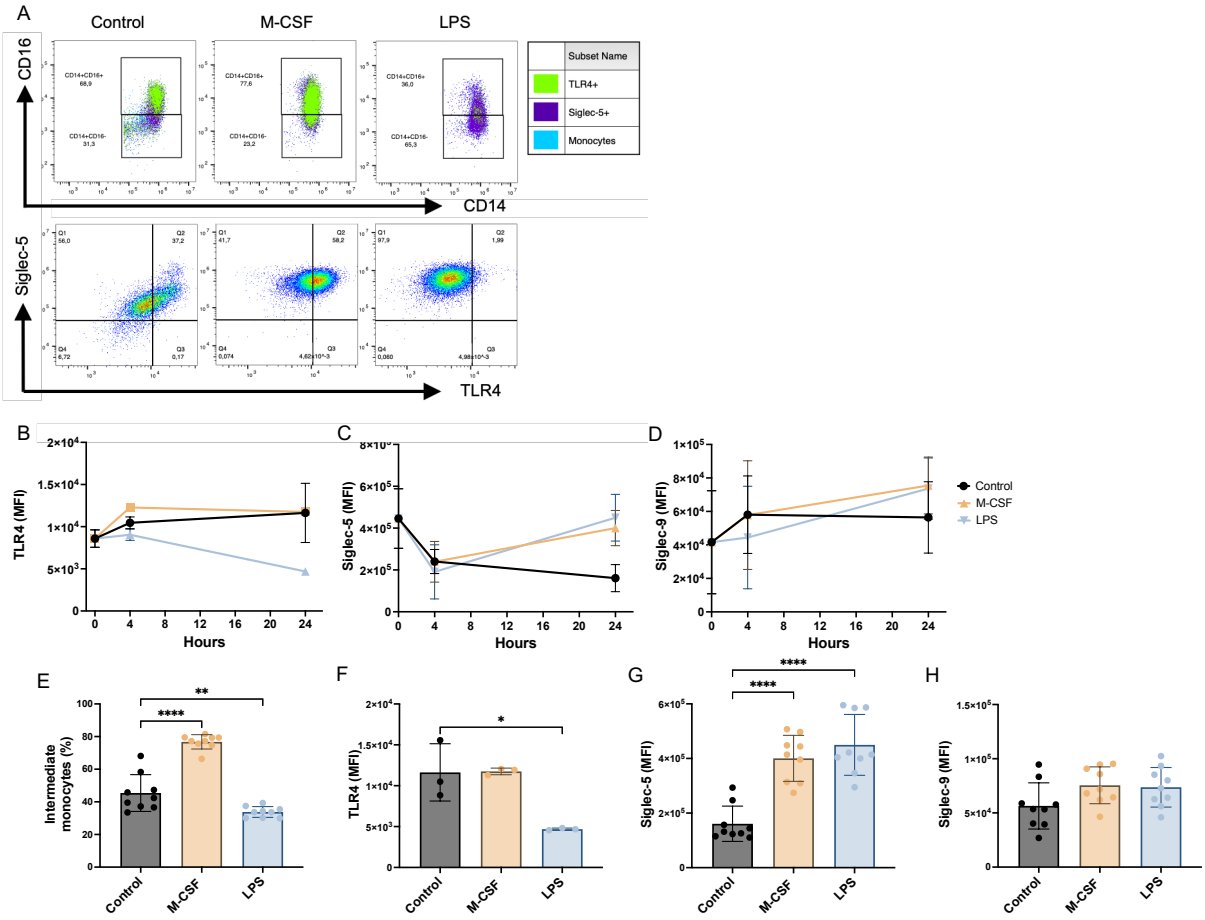

Figure 2. Siglec-5 regulate TLR4 signaling in inflammation

(A) Representative flow cytometric dot plots displaying the percentage classical and intermediate monocytes in the control, and M-CSF- and LPS-stimulated monocytes. Blue represents all cells, green represents TLR4^{+} cells, and purple represents Siglec-5^{+} cells, which can also be displayed in the row of dot plots below.

(B-D) MFI of membrane-associated TLR4, Siglec-5, and Siglec-9 was assessed at 0, 4, and 24hrs of stimulation with M-CSF and LPS, and compared to the control (n = 2-3 from one biological replicate for TLR4, and three biological replicates for Siglec-5 and Siglec-9).

(E) Percentage intermediate monocytes after 24hrs (*n* = 2-3 from three biological replicates).

(F-H) MFI of membrane-associated TLR4, Siglec-5, and Siglec-9 in the control and monocytes stimulated with M-CSF and LPS for 24hrs (*n* = 2-3 from one biological replicate for TLR4, and three biological replicates for Siglec-5 and Siglec-9).

Data is represented as mean±SD, statistical analysis was performed using one-way ANOVA with Dunnett's multiple comparisons test (*p<0.05; **p<0.01; ***p<0.001; ****p<0.0001).

Siglec-5 and TLR4 co-localization on the cell surface of monocytes

Both Siglec-5 and TLR4 are transmembrane receptors which engages extracellularly at the cell-membrane surface as well as interacts with intracellular ligands to induce intracellular

signaling cascades. To understand where the receptors could potentially interact, we performed an in-silico protein-protein prediction in AlphaFold3 for direct contact between TLR4 and Siglec-5 (Figure 3A). [43] For both Siglec-5 and TLR4, a per-residue pLDDT plot identified both confident (70+) secondary structures indicated by blue colors, as well as less confident structures (below 70) indicated by yellow and orange colors. Siglec-5's intracellular domain consisted of intrinsically disordered regions (IDR), making predictions increasingly difficult. When analyzing the output data from the modeling, the predicted aligned error (PAE) in the relative position and orientations of the proteins revealed several potential interaction points between the proteins, both the resulting predicted template modeling (pTM) score of 0.47 and ipTM score of 0.21 indicated low confidence and an overall challenging prediction.
We therefore used immunocytochemistry to investigate the spatial expression patterns and potential physical interactions on monocytes. Representative images show localization of TLR4 (green) and Siglec-5 (red) under each condition (Figure 3B). Both Siglec-5 and TLR4 displayed uniform expression at 0hrs, which changed after 24hrs in culture. As with flow cytometry, a decrease was noted in TLR4 by LPS, whereas Siglec-5 maintained a uniform expression pattern on the cell membrane. At 0hrs, Mander's colocalization coefficient (MCC), determined a strong TLR4 overlap with Siglec-5 (MCC = 0.78), while the more abundantly expressed Siglec-5, as expected, displayed a weak overlap to TLR4 (MCC = 0.35; Figure 3C and 3D). After 24hrs of stimulations, all conditions led to a reduction in TLR4 overlap with Siglec-5, with MCC values ranging between 0.46-0.50, indicating a moderate overlap. Cells stimulated with LPS had lost the correlation between Siglec-5 and TLR4 and now showed no evidence of interaction.

In conclusion, the immunocytochemistry data indicated a potential for these receptors to physically interact on the cell membrane and be regulated by M-CSF and LPS.

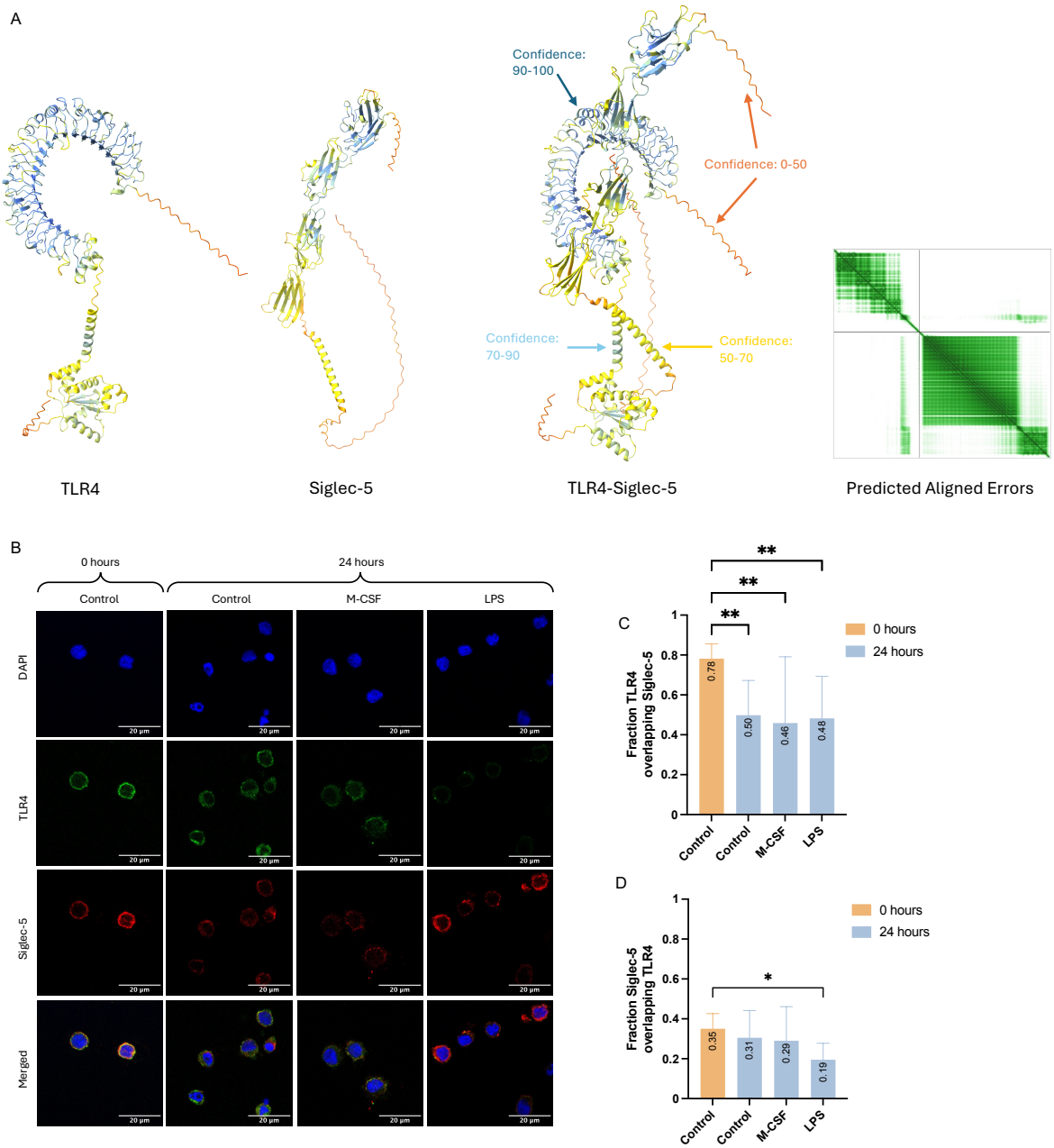

Figure 3. Siglec-5 and TLR4 co-localization on the cell surface of monocytes

(A) The predicted interaction between of TLR4 (O00206) and Siglec-5 (O15389) colored by pLDDT (orange, 0-50; yellow, 50-70; cyan, 70-90; blue, 90-100), were blue indicates high confidence in the prediction and orange color indicates low confidence. The Predicted Alignment Errors (PAE) shows high confidence as green and low confidence as white.

(B) Representative immunofluorescence images of monocytes at baseline, and control, M-CSF, and LPS after 24hrs. Blue color (dapi) colored the nucleus, green color represents TLR4, and red color represents Siglec-5. Scale bar represents 20µm.

(C-D) Mander's colocalization coefficient (MCC) M1: Fraction TLR4 overlapping Siglec-5, and M2: Siglec-5 overlapping TLR4. Data is represented as mean±SD generated from 4-7 images per condition with two biological replicates. Statistical analysis was performed using one-way ANOVA with Dunnett's multiple comparisons test (*p<0.05, **p<0.01).

Intracellular inhibition of TLR4 reduced cytokine secretion and Siglec-5 expression
To assess the functional consequences of Siglec-5 and TLR4 interactions, we measured cytokines produced by the monocytes after the stimulations. To deduce if NFkB signaling was the main signaling pathway involved in the interactions we used the small molecule TLR4 inhibitor TAK-242. This inhibitor specifically binds to Cys747 in the intracellular domain of TLR4, inhibiting both MyD88-dependent and MyD88-independent pathways. [44] The involvement of TLR4-signaling was determined by evaluating how effective TAK-242 was in suppressing cytokine production using a multiplex cytokine screening method. The inhibition was performed prior to the addition of M-CSF, IL1β/TNFα, and LPS and was maintained throughout the experiment.

LPS lead to the most pronounced increase in pro-inflammatory cytokines at both 4hrs (Figure S7A) and 24hrs (Figure 4A). With elevated levels of TNFα, RANTES, IL1β, IL-1ra, MCP-1, IL-10, and G-CSF detected, aligning with its known role to trigger TLR4-mediated inflammation. M-CSF, in contrast, was associated with lower cytokine secretion consistent with its role in differentiation of monocytes into macrophages. Prominent inhibition of cytokine secretion by TAK-242 was observed after LPS as well as with M-CSF stimulation after both 4 and 24 hours. IL1β/TNFα induced cytokine secretion as well, however the TAK-242 inhibitor had no influence on the signaling and levels of cytokines produced, as expected (Figure S8).

Next, we evaluated how blocking TLR4 affected monocyte subsets, including the intermediate population, as well as the receptors TLR4, Siglec-5, and Siglec-9. After 4hrs of stimulation, no significant changes in expression patterns were observed after TAK-242 treatment (Figure S7B-S7E). However, inhibition of TLR4 signaling induced a significant abundance in intermediate monocytes after 24hrs (Figure 4B). TAK-242 only induced significant TLR4 expression after M-CSF activation (Figure 4C). M-CSF and LPS induced the highest levels of Siglec-5 and interestingly, blocking TLR4 significantly reduced Siglec-5 expression in these two groups (Figure 4D). In contrast, Siglec-9 expression remained unchanged when TLR4 was blocked (Figure 4E). TAK-242 had no impact on the fraction TLR4 overlap with Siglec-5 and vice versa (Figure 4F and 4G). These findings suggest that TLR4 inhibition influence Siglec-5 expression.

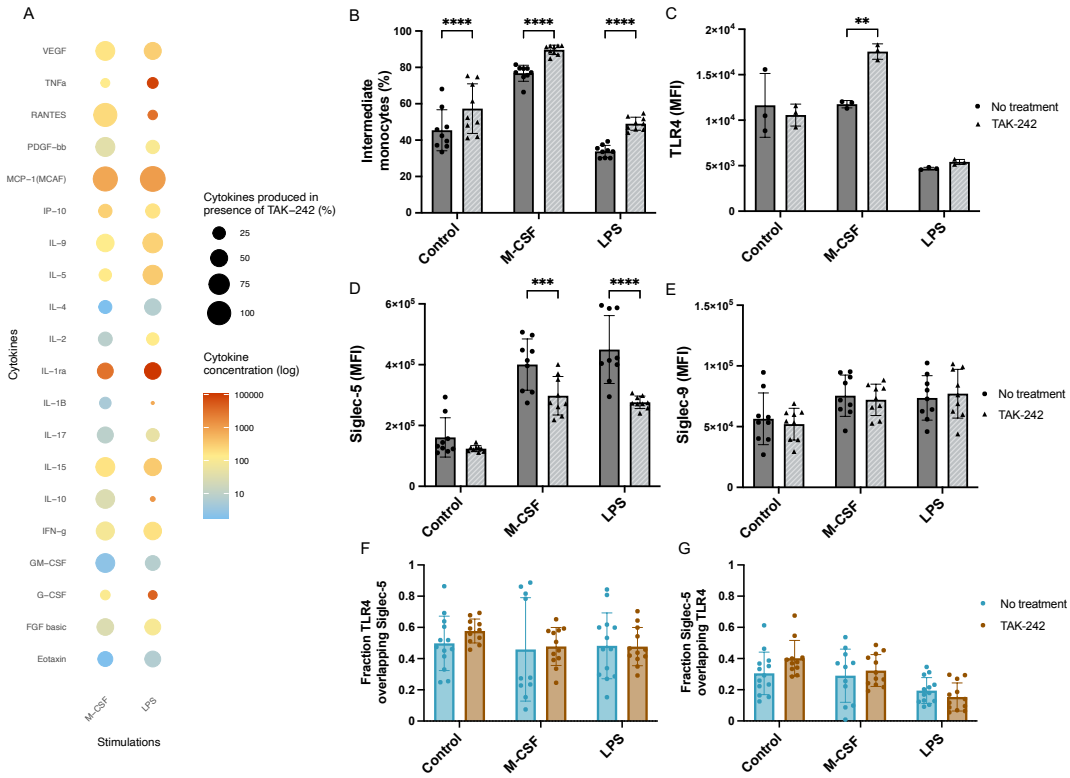

Figure 4. Intracellular inhibition of TLR4 reduced cytokine secretion and Siglec-5 expression

(A) A panel of cytokines and chemokines was screened in the supernatants of monocytes incubated for 24hrs with M-CSF and LPS, with and without the TLR4 inhibitor TAK-242. Each datapoint is the mean of three biological replicates with three technical replicates pooled together. Cytokine levels from monocytes stimulated in absence of TAK-242 is indicated by "Cytokine concentration (log)" and the "Cytokines produced in presence of TAK-242 (%)" indicates how effective TAK-242 was at limiting cytokine secretion compared to without TAK-242.

(B) The percentage of intermediate monocytes after TAK-242 treatment was quantified in monocytes stimulated with M-CSF and LPS and compared to the control at 24hrs (n=2-3 form three biological replicates).

(C-E) The effect of TAK-242 was assessed based on MFI of membrane-associated TLR4, Siglec-5, and Siglec-9 in monocytes stimulated with M-CSF and LPS and compared to the control at 24hrs (n=2-3 form three biological replicates, except TLR4 which was measured in one biological replicate).

(F-G) Mander's colocalization coefficient (MCC) displaying fraction TLR4 overlapping Siglec-5 and vice versa. Each datapoint represents one image, 4-7 images were used per condition from two biological replicates.

Data is represented as mean±SD, statistical analysis was performed using two-way ANOVA with Sidak's multiple comparisons test (*p<0.05; **p<0.01; ***p<0.001; ****p<0.0001).

Siglec-5 and TLR4 interaction is abrogated by loss of sialoglycans

To delineate mechanisms pertaining to Siglec-5 signaling and its correlation to TLR4, sialidase was used to remove membrane-bound Sia and to assess its effect on cell behavior, especially as TLR4 is sialylated. [36] The ability of sialidase to enzymatically remove Sia from glycans was confirmed by LC-MS, where an increased level of O-glycans lacking Sia was detected in sialidase treated monocytes (Figure 5A). TLR4 expression was also shown to be reduced after treatment with sialidase, whereas Siglec-5 displayed similar expression as control (Figure 5B and 5C). The colocalization of TLR4 and Siglec-5 after 24hrs of sialidase treatment was evaluated through immunocytochemistry, which revealed reduced expression of both receptors compared to the control at 0hrs (Figure 5D). The fraction overlap of TLR4 to Siglec-5 (M1), and Siglec-5 to TLR4 (M2) was evaluated using the MCC score (Figure 5E). This revealed a medium TLR4 overlap to Siglec-5 (MCC = 0.47). Similar to LPS, no evidence of overlap between Siglec-5 to TLR4 (MCC = 0.13) was observed. When measuring cytokine production, treatment with sialidase led to an increase in TNFα, RANTES, IL1β, IL-1ra, MCP-1, IL-10, and G-CSF, the same proinflammatory cytokines as LPS induced (Figure 5F).

Inhibition of TLR4 signaling using TAK-242 in cells treated with sialidase seemed to affect TLR4 surface expression but not Siglec-5 (Figure 5B and C). Similar to LPS, TAK-242 treatment of cells treated with sialidase was also effective in limiting cytokine secretion, suggesting that removing extracellular Sia on TLR4 induces both dependent- and independent MyD88 pathways. [44]

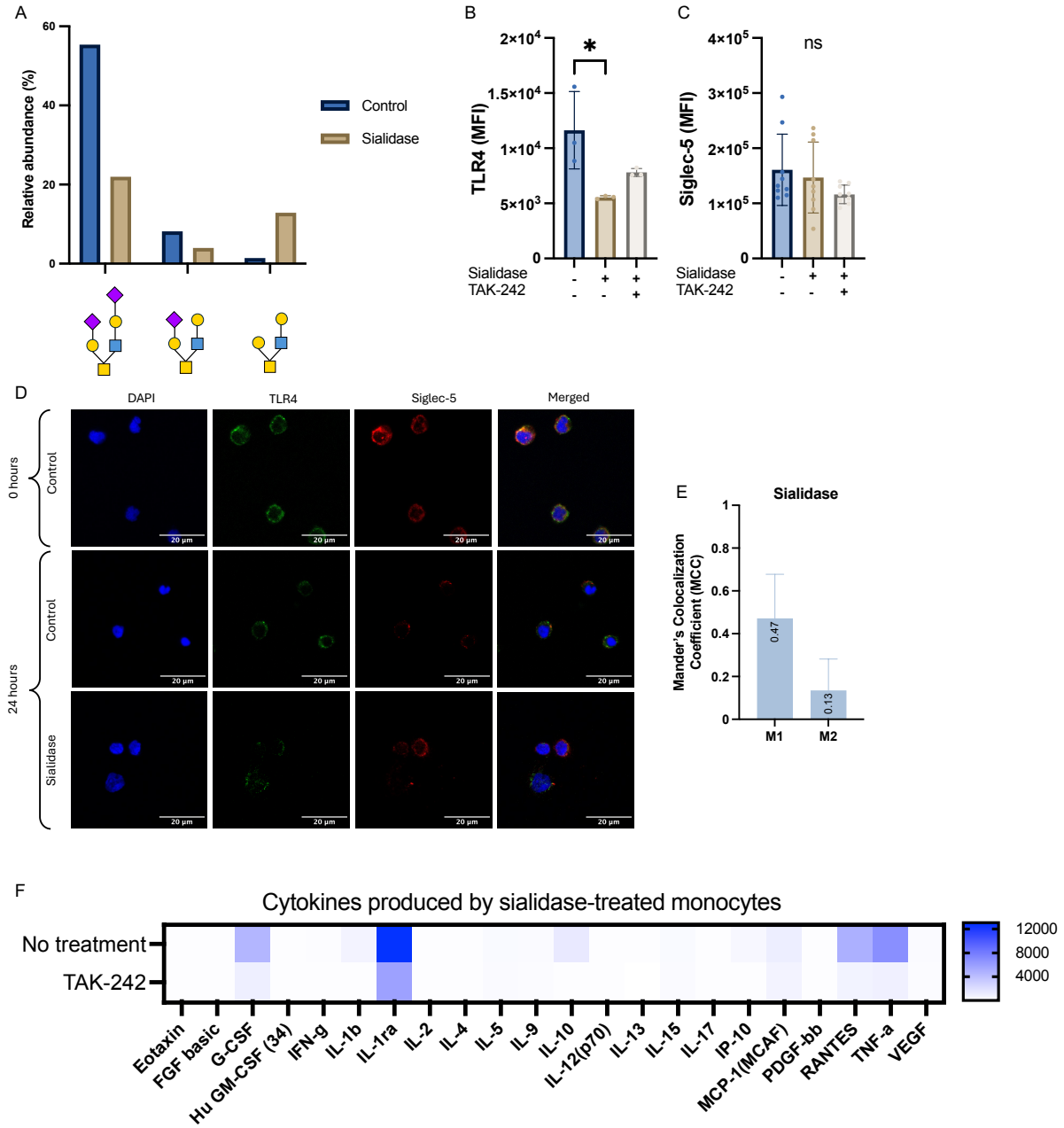

Figure 5. Siglec-5 and TLR4 interaction is abrogated by loss of sialoglycans

(A) Sialidase activity was confirmed using LC-MS, the relative abundance of top two sialylated *O*-glycans and non-sialylated *O*-glycan in control and sialidase treated monocytes was quantified.

(B-C) Monocytes were enzymatically stripped of their membrane-bound Sia for 24hrs in presence or absence of TAK-242 and compared to the control. MFI of membrane-associated TLR4 and Siglec-5 was assessed.

(D) Colocalization of TLR4 and Siglec-5 was investigated in monocytes treated with sialidase for 24hrs compared to the control at 0 and 24hrs.

(E) Manders colocalization coefficient (MCC) M1 and M2, representing "Fraction TLR4 overlapping with Siglec-5" and "Fraction Siglec-5 overlapping with TLR4", respectively.

(F) A panel of cytokines and chemokines was screened in the supernatants of monocytes incubated for 24hrs with sialidase, with and without the TLR4 inhibitor TAK-242. Each datapoint is the mean of three biological replicates with three technical replicates pooled together.

Data is represented as mean±SD, statistical analysis was performed using one-way ANOVA with Dunnett's multiple comparisons test (*p<0.05; **p<0.01; ***p<0.001; ****p<0.0001).

IL-6 secretion levels can be linked to distinct monocyte phenotypes

The secretion of TLR4-dependent IL-6 production induced by sialidase, LPS, and M-CSF, was compared to monocytes stimulated with OA SFs. Sialidase and LPS induced the highest levels of IL-6 and OA SFs induced a low-grade inflammatory profile (Figure 6A).

By understanding how the patient IL-6 profiles corresponded to the phenotypes induced from the Siglec-5 – TLR4 interactions, clustering analysis was performed based on CD14, CD16, TLR4, Siglec-5, and Siglec-9. Uniform Manifold Approximation and Projection (UMAP) dimensionality reduction (Figure 6B) displayed the six distinct monocyte populations generated (Pop1-Pop6), with Pop1 being the largest (71,100 cells) and Pop6 being the smallest (238 cells). Heatmap analysis of marker expression (Figure 6C) revealed that Pop1 was characterized by reduced TLR4/CD16 and increased Siglec-5/CD14 expression. Pop2 displayed the lowest levels of TLR4, accompanied by an induced CD14 expression. Siglec-5 was upregulated in Pop1, 3, 4, and 6. Each condition was displayed as UMAP density contour plots (Figure 6D). Pop1 and Pop4, along with Pop2 were the most abundant subtypes generated in monocytes stimulated with SF1-7, revealing similarities with the low-grade inflammatory profile induced by M-CSF. While monocytes stimulated with SFs displayed a wide distribution of subpopulations, it was evident that SF5 revealed similarities to the higher inflammatory conditions (LPS and sialidase) with a higher abundance of Pop3, Pop5, and Pop6 as well as a higher level of IL-6. These populations displayed the lowest expression of CD16, higher TLR4/CD14, and varying Siglec-5 levels.

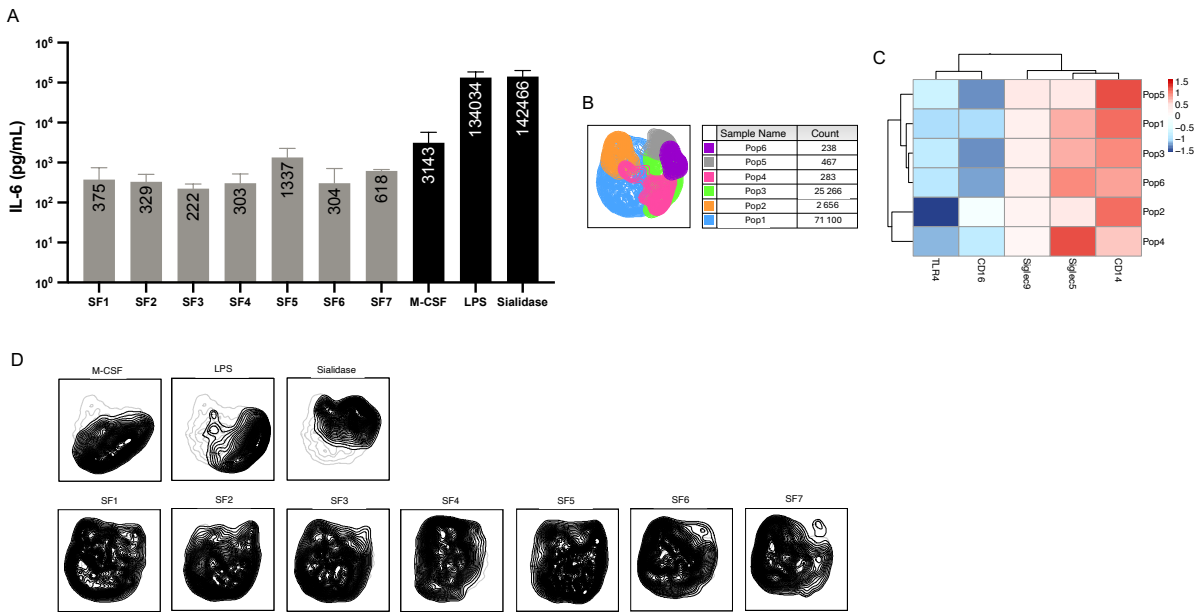

Figure 6. IL-6 secretion levels can be linked to distinct monocyte phenotypes

(A) The concentration of IL-6 (pg/mL) produced by the stimulated monocytes were quantified, grey bars represent SFs, and black bars represent the pathway-specific stimulations. Data is represented as mean±SD, with three technical replicates from three biological replicates.

(B) Analysis was performed on concatenated monocytes stimulated with M-CSF, LPS, sialidase, and SF1-7. Subsequently, monocytes were downsampled to 100,000 cells before performing clustering analysis using the FlowSOM plugin. This generated six monocyte subpopulations, the table displays each population and its count, respectively. For the monocytes stimulated with SF1-7, three technical replicates were used from three biological replicates. For monocytes stimulated with M-CSF, LPS, and sialidase, three technical replicates were used from one biological replicate.

(C) Heatmap analysis demonstrate the six populations and their relative expression of TLR4, CD16, Siglec-9, Siglec-5, and CD14.

(D) Each UMAP contour density plot represents one condition, i.e. M-CSF, LPS, sialidase, and SF1-7.

DISCUSSION

In this study, we identified Siglec-5 as a potential regulatory protein in OA pathogenesis using a unique approach involving NPs. By performing proteomics analysis on the proteins formed around NPs incubated with OA SF, we detected Siglec-5 as one of 14 most abundant proteins. Through the IntAct Molecular Interaction Database, TLR4 was identified as the protein with the highest confidence score to Siglec-5. While the role of TLR4 has been extensively studied in OA, [20] the link to Siglecs remain unclear. We confirmed the regulatory role of Siglec-5 on monocytes by stimulating cells with OA SF, inducing Siglec-5 expression which inversely correlated with TLR4. Mechanistically, we showed that the Siglec-5 – TLR4 interactions are

regulated by sialoglycans on the cell surface, where highly inflammatory cytokines such as those induced by LPS or sialidase, closely mirrored those found in patients with high inflammatory activity. Since TLR4 is increasingly recognized as a key player in age-related diseases like OA, [20,21,25,45] our finding that Siglec-5 can modulate TLR4-driven proinflammatory signaling highlights a potentially unexplored regulatory axis in OA pathogenesis.

Interestingly, we found that OA SF induced Siglec-5 expression which inversely correlated with TLR4 at 24hrs, suggesting potential crosstalk between these receptors. This inverse relationship may reflect a negative feedback mechanism, where Siglec-5 reduces TLR4-driven inflammation in OA, potentially mitigating tissue damage. Siglec-5 has been shown to interact with TLR4, and the murine Siglec-E facilitates TLR4 internalization. [19,30,46] Given that TLR4 is a key driver of proinflammatory activity in OA, [20,45] its regulation by Siglec-5 may serve as an important immunomodulatory checkpoint.
This was further strengthened by the observation that LPS and sialidase significantly reduced TLR4 expression, likely as a desensitization mechanism to prevent monocytes from overreacting to sustained inflammatory stimuli. [47] We investigated potential direct interactions between the two receptors, as TLR4 is known to be heavily sialylated. [36,48] Colocalization analysis revealed a strong overlap at baseline, in line with previous studies suggesting that Siglecs can bind and regulate TLR activity. The high level of IDRs at the membrane interface in both TLR4 and Siglec-5 indicate a tunable interaction surface, one capable of rapid regulation in response to environmental cues, a key feature of immune cell communication. [49]

However, with prolonged stimulations, we observed a progressive reduction in colocalization. Colocalization scores below 0.2 indicated a loss of interaction, suggesting that LPS and sialidase disrupted Siglec-5/TLR4 engagement. This supports a model where the interaction is temporally regulated, strong early on then declining as immune activation progresses. This temporal tuning may serve as a critical checkpoint, allowing for transient modulation of TLR4 signaling during early immune responses while ensuring desensitization under persistent stimulation to prevent tissue damage.
Mechanistically, the loss of interaction appears to stem from depletion of membrane-bound Sia rather than complete receptor downregulation. Surface Sia levels have been directly linked to a cells' maturation state and inflammatory potential, [50,51] and their removal, via sialidase or inflammatory stimuli, may directly influence Siglec binding. Both Siglec and TLR4 expression and activity are modulated by interactions with glycan structures, particularly α2,3 and α2,6 Sia linked Sia residues. These glycan modifications can modulate immune cell signaling and are often altered in response to inflammation [52,53].

The role of Siglec-5 in OA and its exact signaling mechanisms remain poorly understood. Our study found that short-term activation reduced Siglec-5 expression, which was recovered by 24hrs, suggesting either a shedding or internalization mechanism. A recent study on septic patients found elevated levels of soluble Siglec-5 in plasma which could be induced by stimulating monocytes with LPS. [16] Monocytes might hence shed Siglec-5 to modulate other immune cells, explaining why Siglec-5 could be found in high abundance in the proteins

associated with the NPs. It is possible that Siglec-5 plays a role in this desensitization to not exacerbate inflammation. Monocytes stimulated with LPS and sialidase exhibited highly similar cytokine secretion profiles, reflecting their shared activation through TLR4. [35,36,54] Other studies have shown that LPS leads to an overexpression of host sialidase, reducing membrane-bound Sia, and using an exogenous sialidase can thereby mimic LPS stimulation. [55] This functional similarity was further supported by the comparable inhibitory effects observed by TAK-242. Several studies [34,56] have demonstrated changes in surface sialylation in OA chondrocytes and fibroblast-like synoviocytes in rheumatoid arthritis, indicating that inflammation significantly affects glycosylation patterns. [34,56] Our UMAP analysis revealed a wide distribution of both low- and high-grade inflammatory monocytes, with proinflammatory profiles generated by LPS and sialidase. Interestingly, SF5 exhibited an overlap with a high-grade inflammatory profile, correlating with increased IL-6 secretion. Other OA SF-stimulated monocytes shared similarities with M-CSF-stimulated monocytes, consistent with a low-grade inflammation. These findings highlight how interpatient variability influence subtle changes in monocyte surface markers, ultimately shaping inflammatory responses, where Siglecs could play a role in regulation. The high levels of Siglec-5 induced by LPS and contrasting low levels induced by sialidase, indicated that the immunomodulatory effects by Siglec-5 was limited in high-inflammatory conditions within 24hrs. However, in low-grade inflammation, such as with OA SF, patients with higher Siglec-5 expression may have a more tightly controlled immune response, preventing the overactivation of TLR4 signaling and associated inflammation.

We acknowledge some key limitations to our study. While this study has focused on monocytes, many different cells are involved in OA, including chondrocytes and synoviocytes. Modulation of $CD8^+$ T-cell proliferation by soluble Siglec-5, [16] suggests Siglec-5 could have potential autocrine effects on other OA-related cells. The transient increases in Siglec-5, alongside persistent decreases in the sialidase group, suggest ongoing glycan remodeling that may involve TLR4 or other receptors. Longer observation periods and dose-dependent studies, particularly with sialidase, are needed to clarify these dynamics. Broader investigation into glycosylation patterns and their impact on immune receptor networks could uncover additional therapeutic targets. Future work should also validate these findings in vivo and in human OA samples, focusing on how sialylation patterns and Siglec-5 expression vary among patient subgroups.

In conclusion, this study highlights the role of Siglec-5 on TLR4 in the pathogenesis of OA, shedding light on their intricate interplay. While both Siglec-5 and TLR4 are implicated in the inflammatory process of OA, their complex relationship warrants further investigation to fully elucidate the underlying mechanisms and interactions. The dynamic interplay between glycosylation, receptor localization, and immune signaling could in the future be validated using proximity ligation assays, live cell imaging or co-immunoprecipitation could further clarify the spatial and temporal nature of this interaction, while lectin-based profiling could confirm changes in Sia presentation. The marked reduction in cytokine production upon TLR4 inhibition underscores the therapeutic potential of TAK-242 particularly for patient subgroups with low Siglec-5 or skewed Sia expression, where modulation of TLR4 signaling

may prove especially beneficial. Similar features imposed on monocytes by LPS and sialidase demonstrated TLR4-specific activation. Yet, sialidase failed to upregulate Siglec-5, emphasizing an important role of Sia as ligand which could serve as a potential therapeutic target for immune cell modulation. Restoring Siglec-5 function and understanding its signaling mechanisms presents promising opportunities to modulate TLR4 signaling and reduce inflammation not only in OA, but for many pathogeneses where modulating glycosylation patterns can be used to fine-tune immune responses.

MATERIALS AND METHODS

Sex as a biological variable

This study includes patient material from both female and male patients. Synovial fluid from 7 OA patients (2 females) due for total knee replacement surgery was selected for the experiments: age 63-87 (Median 77) and BMI 23.4-38.0 (Median 25.6). Due to the small patient population, no further stratification was made. To remove cells from OA SF, it was centrifuged at 3000 x g for 10 min before storing at -80°C.

Protein corona isolation and material synthesis

NP synthesis was previously described in von Mentzer *et al.* [10] Briefly, PAMAM (G5) were modified by PEGylation using PEG 350 MW, NP_{350} at 2%, or PEG 5000 MW, NP_{5000} at 2%, purified, and used at the final concentration of 30 µM in PBS (pH = 7.4).

SF samples from 4 (2f/2m, 45–82 years old) late OA patients were collected during aseptic aspiration of knee joints at the Rheumatology Clinic and Orthopaedic Clinic, respectively, at Sahlgrenska University Hospital, Gothenburg, Sweden.
Patient SF were pooled, diluted 1:20 in PBS, and mixed with 30 µM NP solution (1:1, v/v). The samples were incubated at 37°C while shaking for 1 h at 100 rpm to resemble the dynamic environment of the SF in the joint and address the Vroman effect. To preserve the proteins bound with high affinity known as the hard protein coronas, NPs were spun down at 15,000 × *g* for 15 min and washed three times with chilled PBS. Final concentration of NP-protein complexes was 1 µg/mL (2.5×10^8 particles/mL).

NPs were pelleted by centrifugation at 15,000 × *g* for 15 min, snap-frozen using liquid nitrogen, and submitted to the Proteomics Core Facility (Gothenburg, Sweden). Briefly, proteins were digested into peptides using MS-grade trypsin and analyzed by nanoscale liquid chromatography-tandem mass spectrometry LC-MS/MS. The mascot search engine was used to match the discovered peptide sequences against SwissProt human and bovine protein database using Proteome Discoverer. Data were analyzed using a label-free quantification method and the protein false discovery rate was set to 1%. To elucidate the molecular functions and classifications of significant proteins, the enrichment analysis was performed using Gene Ontology-based PANTHER classification system. SF samples were matched to

human (Homo sapiens). The detected proteins were analyzed and illustrated as a volcano plot using the DEP R package as described in. [10]

Monocyte isolation

Buffy coats obtained from anonymous healthy donors from the blood bank at Sahlgrenska University Hospital, Gothenburg, Sweden (18/23) were prepared the day before and collected for the experimental study in the morning. Monocyte isolation was performed using the negative selection RosettSep™ Human Monocyte Enrichment Cocktail (Stemcell Technologies). Since this kit is optimized for whole blood, the buffy coat was diluted 1:1 with Dulbecco's phosphate buffered saline (PBS) (Gibco) to ensure that the concentration of nucleated cells did not exceed the limit. Apart from that, the isolation was performed according to the protocol. Briefly, the blood was mixed with the cocktail and incubated for 20 min at room temperature. Following this, the mixture was placed over a Ficoll-Paque (Cytiva) density gradient medium and centrifuged in a swing-out bucket for 20 min at 1200 x g with the brake off. The enriched monocytes were transferred to a new tube and washed in the recommended medium containing PBS, 2% heat inactivated fetal bovine serum (FBS, Gibco, Paisley, UK), and 1mM EDTA (Thermo-fisher). After this, the monocytes were washed twice in recommended medium and centrifuged at 300 x g for 10 min with the brake low.

Monocyte stimulations

The enriched monocytes were counted and plated at a concentration of 3 x 10^5 cells/well in a 48 well plate (Costar). The cells were diluted in RPMI Medium 1640 (Gibco, Paisley, UK) supplemented with 1 % glutaMAX (Gibco, Grand Island, USA), 1 % Penicillin/Streptomycin and 10 % FBS. TAK-242 (Merck) was added to the designated wells at a concentration of 1µM and incubated for one hour. The final concentration of each stimulation was 10ng/mL of IL1β and TNFα, 100ng/mL M-CSF, 100ng/mL LPS, and 100mU/mL sialidase (Sigma-Aldrich, N2876). The cells were analyzed after 0, 4, and 24 hours.
As a comparison to these commonly used stimulations, we incubated primary monocytes with OA synovial fluid at a concentration of 25%. After 24hrs of stimulation the surface markers were detected using flow cytometry.

Cell staining for flow cytometric analysis

Monocytes were collected by transferring the whole volume to a v-plate (Costar) and centrifuging them at 300 x g for 5 minutes, 4°C. The supernatants were transferred and saved at -80°C for cytokine measurement. Meanwhile, to detach the monocytes that started differentiating into macrophages, 50µL trypsin-EDTA (Gibco) was added. Once detached, 50µL ice cold recommended medium was used to inactivate trypsin. The detached cells were added to the v-plate and washed twice. 10µL Fc block (Biolegend) was added to each well and the plate was incubated on ice for 10 min. Monocyte phenotypes were analyzed using the following antibodies at a final concentration of 1:100, CD14-FITC, CD16-Brilliant Violet 605, Siglec-5-PE, Siglect-9-PE-Cy7, and TLR4-APC (Biolegend). 10µL the antibody cocktail was added to each well and the plate was incubated for 20 min on ice in the dark. The cells were washed three times in recommended medium. To exclude dead cells, 1µM DAPI (Biolegend) was added. Fluorescence minus one (FMO) and unstained cells were used to set

up the gating. The cells were run on the Cytoflex LX (Beckman Coulter), median fluorescence intensity (MFI) was recorded and analyzed using FlowJo (Version 10.10.0).

Clustering and nonlinear dimensionality reduction

Unsupervised analysis was performed using FlowJo. Cells from all stimulations (SF1-SF7 and M-CSF, LPS, and sialidase) were concatenated into one single file. Clustering was conducted using the FlowSOM plugin, generating six distinct populations. Subsequently, a UMAP was generated based on these populations. For visualization, each stimulation condition was overlaid onto separate UMAPs to illustrate the distribution of populations across each stimulation.

LC-MS

After isolating monocytes, they were diluted to a concentration of 2 x 10^6 cells and added to two Eppendorf tubes. Sialidase was added so that the number of units was the same as in the experiments, the tubes were incubated for 1 hour at 37°C. The tubes were centrifuged at 2500 x g for 10 min at 4°C. Supernatant was removed, the same washing step was performed two more times. Subsequently, 100µL lysis buffer (PBS + 2% SDS) was added, the tubes were briefly sonicated followed by gentle shaking for 10 min. Cell debris was removed by centrifugation at 14000 x g for 20 min. The supernatant was collected, and the protein concentration was measured using gold-standard BCA assay. Approximately 30 µg of extracted protein samples were dot blotted on a PVDF membrane (Millipore). Proteins were stained using Alcian blue stain solution, excised and transferred to an Eppendorf tube. O-glycans were released and analyzed on liquid chromatography and mass spectrometry according to this protocol. In short, the dot blotted proteins were subjected to reductive β-elimination with 0.5 M sodium borohydride in 50 mM sodium hydroxide for 16 h at 50°C to release the glycans. The reduction reaction was quenched by the addition of glacial acetic acid and the resulting glycan containing mixtures were desalted using strong cation exchange resin packed on top of C18 column to remove the remaining proteins or peptides. The released glycans were analyzed using liquid chromatography and mass spectrometry. The glycans were separated on a column (10 cm × 250 µm) packed in-house with 5 µm porous graphite particles (PGC, Hypercarb, Thermo-Hypersil, Runcorn, UK) and at a flow rate of 6 µl/min. The samples were analyzed in negative ion mode on an Orbitrap mass spectrometer (Fusion, Thermo Electron, San José, CA) and the data acquisition was conducted with Xcalibur software (Version 2.0.7).

Bio-Plex Pro Human Cytokine Grp I Panel 27-Plex

Supernatants from the monocyte stimulation assays were screened for a panel of 27 cytokines and chemokines to evaluate the immune response in the different conditions. The technical replicates from three biological replicates were combined, respectively, to reduce the number of wells to one well per biological replicate. The assay was performed according to the manufacturer's instructions. Briefly, vortexed beads were added to each well, followed by two washing steps. Samples were centrifuged at 1,000 x g for 15 min at 4°C prior being added to the plate along with the standard, blank, and control. The plate was incubated shaking at 850 rpm for 30 min, followed by three washing steps. Detection antibodies were added to each

well and incubated shaking for 30 min. After three washings, streptavidin-PE was added and incubated shaking for 10 min. An additional three washings were performed before resuspending the beads in assay buffer and reading the plate.
For values that were out of range, extrapolated values were assumed based on the highest and lowest value of the standard curve. We observed that most of the groups was below detection level for IL-7 and above detection level for MIP-1α, MIP-1β, IL-6, and IL-8 and they were hence removed. Additionally, the media control was below detection level for most analytes and thus removed.

The cytokines detected were normalized in Prism (GraphPad software Version 10.4.1 (532)). For each subcolumn, values were scaled as fractions, with 0% representing smallest value of each sub column, and 100% represents the sum of all values in the subcolumn. The ggplot2 R[57] package was used to create the dot plot heatmap illustrating cytokine expression under different stimulation conditions, along with the percentage cytokines remaining in presence of TAK-242.

Confocal microscopy
To analyze TLR4 and Siglec-5 colocalization, confocal imaging was performed. $1.2x10^6$ isolated monocytes were seeded in complete RPMI in 12 well plates and pre-treated with 1µM TAK-242 or PBS, for 1 hour. Following this, the stimulations M-CSF, LPS, and Sialidase were added accorded to previously mentioned concentrations. After 0 and 24h, the monocytes were transferred to Eppendorf tubes and the leftover attached cells were trypsinized and transferred to the tubes before being centrifuged at 1,500 rpm for 5 min. The supernatant was discarded, and the cells were washed with PBS and centrifuged to remove the supernatant, this was performed three times. To fix the cells, 100µL 4% paraformaldehyde (PFA) was added to each tube and incubated at room temperature for 10 min. Detection was performed using anti-human TLR4 mouse monoclonal antibody (HTA-125, Invitrogen) and anti-human Siglec-5 rabbit polyclonal antibody (13230-1-AP, Proteintech), both diluted 1:100 and stained for 1h in room temperature. 2 µg/mL of secondary antibody goat anti-mouse IgG (A32723, Thermo Fisher) and goat anti-rabbit IgG (A21245, Thermo Fisher) was incubated in the dark for 1h. After washing, the cells were spun onto a glass slide, ProLong™ Gold Antifade Mountant (Invitrogen) was added before mounting the cover slip. Images were acquired by using an inverted Nikon C2+ confocal microscope (Nikon Instruments, Amsterdam, Netherlands) equipped with a C2-DUVB GaAsP detector unit offering variable emission bandpass settings. A 60x Nikon APO oil-immersion objective (numerical aperture 1.4). Excitation and emission were set as follows for different staining: DAPI - λ_{ex} 401 nm, λ_{em} 425-497 nm, goat anti-rabbit IgG (Alexa Fluor 647) - λ_{ex} 639 nm, λ_{em} 644-695 nm, and goat anti-mouse IgG (Alexa Fluor 488) - λ_{ex} 489 nm, λ_{em} 503-546 nm.

Image analysis
The confocal images displayed in Figure 4A were enhanced for illustrative purposes. The brightness was equally enhanced for TLR4 and Siglec-5, for accurate comparison. Mander's colocalization coefficient (MMC) was performed on unaltered images. Threshold was set to

90 for TLR4 and 140 for Siglec-5 to remove background. All controls demonstrated 0 overlap. MCC was calculated through the JACoP plugin in ImageJ2 (Version 2.16.0/1.54p).

R packages

Figure 1B, Figure 4A, Figure 6C, and Figure S7A were created in Rstudio (R version 4.3.2 (2023-10-31). The following packages were used: readr, tidyverse, igraph, ggraph, ggplot2, and scales.[58-64]

Statistics

Statistical significance was performed using Prism (GraphPad software Version 10.4.1 (532)). Data are shown as the mean and standard deviation and statistical differences were analyzed using One-way ANOVA followed by Tukey's or Dunnett's multiple comparisons test or two-way ANOVA followed by Sidak's multiple comparisons test. Correlation was analyzed using Spearman correlation analysis. All statistical details can be obtained in the figure legends.

Study approval

The studies involving human participants were reviewed and approved by the Regional Ethical Review Board in Gothenburg. All patients provided informed consent, and the procedure was approved by the Ethics Committee of Gothenburg University (Ethical approval Dnr: 573-07, 172-15).

Data availability

The original contributions presented in the study are included in the article or Supplemental Material; further inquiries can be directed to the corresponding author.

Author Contributions

Study design (L.R, A.S), conducting experiments (L.R, F.J, U.v.M, V.V), acquiring data (L.R, F.J, U.v.M, V.V), analyzing data (L.R, F.J, U.v.M, V.V, A.S), providing funding and reagents (N.K, A,S), writing the manuscript (L.R, A.S). All authors have contributed to editing and approved the manuscript.

Declaration of interest: NK authored a patent involving OA diagnostics, and NK hold equity in Lynxon AB. The other authors have declared that no conflict of interest exists.

Acknowledgements:

Anna-Karin Hultgård-Ekwall, Lena Björkman, Thomas Eisler, and Ola Rolfson are gratefully acknowledged for arranging the patient samples, and Sofia Grindberg and Paula-Therese Kelly Pettersson at Danderyd's Hospital and Lotta Falkendahl at the University of Gothenburg are acknowledged for their assistance in collecting the samples. This work was supported by Chalmers Technical University and its Area of Advance Nano. The authors greatly acknowledge further financial support from the Foundation for Sigurd and Elsa Goljes Minne (LA2021-0100), The Royal Swedish Academy of Sciences (CR2021-0024), The Jeanssons Foundation (J2021-0050), The Hasselblad Foundation, the Swedish Research Council (2021-01870), Wilhelm och Martina Lundgrens Vetenskapsfond (2022-4054) the Swedish

Rheumatism Association (R-981253), the King Gustav V's 80 years' foundation (FAI-2022-0872) and IngaBritt och Arne Lundbergs Forskningsstiftelse (LU2022-0041).

Declaration of generative AI and AI-assisted technologies in the writing process
During the preparation of this work, we used OpenAI for language editing and to ensure readability. After using this tool/service, we reviewed and edited the content and take full responsibility for the content of the published article.

References

1. Courties, A., Kouki, I., Soliman, N., Mathieu, S., and Sellam, J. (2024). Osteoarthritis year in review 2024: Epidemiology and therapy. Osteoarthritis Cartilage *32*, 1397-1404. 10.1016/j.joca.2024.07.014.
2. Ye, Z., Wang, Y., Xiang, B., Wang, H., Tao, H., Zhang, C., Zhang, S., Sun, D., Luo, F., and Song, L. (2023). Roles of the Siglec family in bone and bone homeostasis. Biomed Pharmacother *165*, 115064. 10.1016/j.biopha.2023.115064.
3. Zhang, H., Cai, D., and Bai, X. (2020). Macrophages regulate the progression of osteoarthritis. Osteoarthritis and Cartilage *28*, 555-561. 10.1016/j.joca.2020.01.007.
4. Zhu, X., Lee, C.-W., Xu, H., Wang, Y.-F., Yung, P.S.H., Jiang, Y., and Lee, O.K. (2021). Phenotypic alteration of macrophages during osteoarthritis: a systematic review. Arthritis Research & Therapy *23*. 10.1186/s13075-021-02457-3.
5. Yin, X., Wang, Q., Tang, Y., Wang, T., Zhang, Y., and Yu, T. (2024). Research progress on macrophage polarization during osteoarthritis disease progression: a review. Journal of Orthopaedic Surgery and Research *19*. 10.1186/s13018-024-05052-9.
6. Kloppenburg, M., Peterfy, C., Haugen, I.K., Kroon, F., Chen, S., Wang, L., Liu, W., Levy, G., Fleischmann, R.M., Berenbaum, F., et al. (2019). Phase IIa, placebo-controlled, randomised study of lutikizumab, an anti-interleukin-1α and anti-interleukin-1β dual variable domain immunoglobulin, in patients with erosive hand osteoarthritis. Annals of the Rheumatic Diseases *78*, 413-420. 10.1136/annrheumdis-2018-213336.
7. Yu, L., Luo, R., Qin, G., Zhang, Q., and Liang, W. (2023). Efficacy and safety of anti-interleukin-1 therapeutics in the treatment of knee osteoarthritis: a systematic review and meta-analysis of randomized controlled trials. Journal of Orthopaedic Surgery and Research *18*. 10.1186/s13018-023-03590-2.
8. Zhu, R., Fang, H., Wang, J., Ge, L., Zhang, X., Aitken, D., and Cai, G. (2024). Inflammation as a therapeutic target for osteoarthritis: A literature review of clinical trials. Clinical Rheumatology *43*, 2417-2433. 10.1007/s10067-024-07042-y.
9. Morici, L., Allémann, E., Rodríguez-Nogales, C., and Jordan, O. (2024). Cartilage-targeted drug nanocarriers for osteoarthritis therapy. Int J Pharm *666*, 124843. 10.1016/j.ijpharm.2024.124843.
10. von Mentzer, U., Sellden, T., Raberg, L., Erensoy, G., Hultgard Ekwall, A.K., and Stubelius, A. (2022). Synovial fluid profile dictates nanoparticle uptake into cartilage - implications of the protein corona for novel arthritis treatments. Osteoarthritis Cartilage *30*, 1356-1364. 10.1016/j.joca.2022.07.002.
11. Vuchkovska, A., Glanville, D.G., Scurti, G.M., Nishimura, M.I., White, P., Ulijasz, A.T., and Iwashima, M. (2022). Siglec-5 is an inhibitory immune checkpoint molecule for human T cells. Immunology *166*, 238-248. 10.1111/imm.13470.
12. Läubli, H., Nalle, S.C., and Maslyar, D. (2022). Targeting the Siglec–Sialic Acid Immune Axis in Cancer: Current and Future Approaches. Cancer Immunology Research *10*, 1423-1432. 10.1158/2326-6066.cir-22-0366.

13. Lustig, M., Chan, C., Jansen, J.H.M., Bräutigam, M., Kölling, M.A., Gehlert, C.L., Baumann, N., Mester, S., Foss, S., Andersen, J.T., et al. (2023). Disruption of the sialic acid/Siglec-9 axis improves antibody-mediated neutrophil cytotoxicity towards tumor cells. Frontiers in Immunology *14*. 10.3389/fimmu.2023.1178817.
14. Wang, X., Liu, D., Ning, Y., Liu, J., Wang, X., Tu, R., Shen, H., Chen, Q., and Xiong, Y. (2017). Siglec-9 is upregulated in rheumatoid arthritis and suppresses collagen-induced arthritis through reciprocal regulation of Th17-/Treg-cell differentiation. Scand J Immunol *85*, 433-440. 10.1111/sji.12543.
15. Dou, C., Zhen, G., Dan, Y., Wan, M., Limjunyawong, N., and Cao, X. (2022). Sialylation of TLR2 initiates osteoclast fusion. Bone Research *10*, 24. 10.1038/s41413-022-00186-0.
16. Lozano-Rodríguez, R., Avendaño-Ortíz, J., Montalbán-Hernández, K., Ruiz-Rodríguez, J.C., Ferrer, R., Martín-Quirós, A., Maroun-Eid, C., González-López, J.J., Fàbrega, A., Terrón-Arcos, V., et al. (2023). The prognostic impact of SIGLEC5-induced impairment of CD8+ T cell activation in sepsis. eBioMedicine *97*, 104841. 10.1016/j.ebiom.2023.104841.
17. Kukan, E.N., Fabiano, G.L., and Cobb, B.A. (2024). Siglecs as modulators of macrophage phenotype and function. Semin Immunol *73*, 101887. 10.1016/j.smim.2024.101887.
18. Matsumoto, T., Takahashi, N., Kojima, T., Yoshioka, Y., Ishikawa, J., Furukawa, K., Ono, K., Sawada, M., Ishiguro, N., and Yamamoto, A. (2016). Soluble Siglec-9 suppresses arthritis in a collagen-induced arthritis mouse model and inhibits M1 activation of RAW264.7 macrophages. Arthritis Res Ther *18*, 133. 10.1186/s13075-016-1035-9.
19. Wu, Y., Ren, D., and Chen, G.-Y. (2016). Siglec-E Negatively Regulates the Activation of TLR4 by Controlling Its Endocytosis. The Journal of Immunology *197*, 3336-3347. 10.4049/jimmunol.1600772.
20. Bartels, Y.L., Van Lent, P.L.E.M., Van Der Kraan, P.M., Blom, A.B., Bonger, K.M., and Van Den Bosch, M.H.J. (2024). Inhibition of TLR4 signalling to dampen joint inflammation in osteoarthritis. Rheumatology *63*, 608-618. 10.1093/rheumatology/kead493.
21. Kim, H.-J., Kim, H., Lee, J.-H., and Hwangbo, C. (2023). Toll-like receptor 4 (TLR4): new insight immune and aging. Immunity & Ageing *20*. 10.1186/s12979-023-00383-3.
22. Rapp, A.E., and Zaucke, F. (2023). Cartilage extracellular matrix-derived matrikines in osteoarthritis. Am J Physiol Cell Physiol *324*, C377-C394. 10.1152/ajpcell.00464.2022.
23. von Mentzer, U., Corciulo, C., and Stubelius, A. (2022). Biomaterial Integration in the Joint: Pathological Considerations, Immunomodulation, and the Extracellular Matrix. Macromol Biosci *22*, e2200037. 10.1002/mabi.202200037.
24. Huang, S., Thomsson, K.A., Jin, C., Ryberg, H., Das, N., Struglics, A., Rolfson, O., Björkman, L.I., Eisler, T., Schmidt, T.A., et al. (2022). Truncated lubricin glycans in osteoarthritis stimulate the synoviocyte secretion of VEGFA, IL-8, and MIP-1α: Interplay between O-linked glycosylation and inflammatory cytokines. Frontiers in Molecular Biosciences *9*. 10.3389/fmolb.2022.942406.
25. Gómez, R., Villalvilla, A., Largo, R., Gualillo, O., and Herrero-Beaumont, G. (2015). TLR4 signalling in osteoarthritis—finding targets for candidate DMOADs. Nature Reviews Rheumatology *11*, 159-170. 10.1038/nrrheum.2014.209.
26. Barreto, G., Senturk, B., Colombo, L., Brück, O., Neidenbach, P., Salzmann, G., Zenobi-Wong, M., and Rottmar, M. (2020). Lumican is upregulated in osteoarthritis and contributes to TLR4-induced pro-inflammatory activation of cartilage degradation and

macrophage polarization. Osteoarthritis and Cartilage *28*, 92-101. 10.1016/j.joca.2019.10.011.
27. Barreto, G., Manninen, M., and K. Eklund, K. (2020). Osteoarthritis and Toll-Like Receptors: When Innate Immunity Meets Chondrocyte Apoptosis. Biology *9*, 65. 10.3390/biology9040065.
28. Tsuno, H., Tanaka, N., Naito, M., Ohashi, S., Iwasawa, M., Kadoguchi, T., Mitomi, H., Matsui, T., Furukawa, H., and Fukui, N. (2023). Analysis of proteins released from osteoarthritic cartilage by compressive loading. Scientific Reports *13*. 10.1038/s41598-023-45472-x.
29. Warmink, K., Vinod, P., Korthagen, N.M., Weinans, H., and Rios, J.L. (2023). Macrophage-Driven Inflammation in Metabolic Osteoarthritis: Implications for Biomarker and Therapy Development. International Journal of Molecular Sciences *24*, 6112. 10.3390/ijms24076112.
30. Chen, G.Y., Brown, N.K., Wu, W., Khedri, Z., Yu, H., Chen, X., van de Vlekkert, D., D'Azzo, A., Zheng, P., and Liu, Y. (2014). Broad and direct interaction between TLR and Siglec families of pattern recognition receptors and its regulation by Neu1. Elife *3*, e04066. 10.7554/eLife.04066.
31. Feng, C., Stamatos, N.M., Dragan, A.I., Medvedev, A., Whitford, M., Zhang, L., Song, C., Rallabhandi, P., Cole, L., Nhu, Q.M., et al. (2012). Sialyl residues modulate LPS-mediated signaling through the Toll-like receptor 4 complex. PLoS One *7*, e32359. 10.1371/journal.pone.0032359.
32. Wang, T., Hao, Z., Liu, C., Yuan, L., Li, L., Yin, M., Li, Q., Qi, Z., and Wang, Z. (2020). MiR-193b modulates osteoarthritis progression through targeting ST3GAL4 via sialylation of CD44 and NF-κB pathway. Cell Signal *76*, 109814. 10.1016/j.cellsig.2020.109814.
33. Liang, F., Seyrantepe, V., Landry, K., Ahmad, R., Ahmad, A., Stamatos, N.M., and Pshezhetsky, A.V. (2006). Monocyte Differentiation Up-regulates the Expression of the Lysosomal Sialidase, Neu1, and Triggers Its Targeting to the Plasma Membrane via Major Histocompatibility Complex Class II-positive Compartments. Journal of Biological Chemistry *281*, 27526-27538. 10.1074/jbc.m605633200.
34. Carpintero-Fernandez, P., Varela-Eirin, M., Lacetera, A., Gago-Fuentes, R., Fonseca, E., Martin-Santamaria, S., and Mayan, M.D. (2020). New Therapeutic Strategies for Osteoarthritis by Targeting Sialic Acid Receptors. Biomolecules *10*, 637. 10.3390/biom10040637.
35. Allendorf, D.H., Franssen, E.H., and Brown, G.C. (2020). Lipopolysaccharide activates microglia via neuraminidase 1 desialylation of Toll-like Receptor 4. Journal of Neurochemistry *155*, 403-416. 10.1111/jnc.15024.
36. Karmakar, J., Roy, S., and Mandal, C. (2019). Modulation of TLR4 Sialylation Mediated by a Sialidase Neu1 and Impairment of Its Signaling in Leishmania donovani Infected Macrophages. Frontiers in Immunology *10*. 10.3389/fimmu.2019.02360.
37. Barreto, G., Sandelin, J., Salem, A., Nordström, D.C., and Waris, E. (2017). Toll-like receptors and their soluble forms differ in the knee and thumb basal osteoarthritic joints. Acta Orthopaedica *88*, 326-333. 10.1080/17453674.2017.1281058.
38. Huang, Z.Y., Perry, E., Huebner, J.L., Katz, B., Li, Y.-J., and Kraus, V.B. (2018). Biomarkers of inflammation – LBP and TLR— predict progression of knee osteoarthritis in the DOXY clinical trial. Osteoarthritis and Cartilage *26*, 1658-1665. 10.1016/j.joca.2018.08.005.
39. Villaveces, J.M., Jimenez, R.C., Porras, P., Del-Toro, N., Duesbury, M., Dumousseau, M., Orchard, S., Choi, H., Ping, P., Zong, N.C., et al. (2015). Merging and

scoring molecular interactions utilising existing community standards: tools, use-cases and a case study. Database *2015*, bau131-bau131. 10.1093/database/bau131.
40. Gómez-Aristizábal, A., Gandhi, R., Mahomed, N.N., Marshall, K.W., and Viswanathan, S. (2019). Synovial fluid monocyte/macrophage subsets and their correlation to patient-reported outcomes in osteoarthritic patients: a cohort study. Arthritis Research & Therapy *21*. 10.1186/s13075-018-1798-2.
41. Kapellos, T.S., Bonaguro, L., Gemünd, I., Reusch, N., Saglam, A., Hinkley, E.R., and Schultze, J.L. (2019). Human Monocyte Subsets and Phenotypes in Major Chronic Inflammatory Diseases. Frontiers in Immunology *10*. 10.3389/fimmu.2019.02035.
42. Williams, H., Mack, C., Baraz, R., Marimuthu, R., Naralashetty, S., Li, S., and Medbury, H. (2023). Monocyte Differentiation and Heterogeneity: Inter-Subset and Interindividual Differences. International Journal of Molecular Sciences *24*, 8757. 10.3390/ijms24108757.
43. Abramson, J., Adler, J., Dunger, J., Evans, R., Green, T., Pritzel, A., Ronneberger, O., Willmore, L., Ballard, A.J., Bambrick, J., et al. (2024). Accurate structure prediction of biomolecular interactions with AlphaFold 3. Nature *630*, 493-500. 10.1038/s41586-024-07487-w.
44. Takashima, K., Matsunaga, N., Yoshimatsu, M., Hazeki, K., Kaisho, T., Uekata, M., Hazeki, O., Akira, S., Iizawa, Y., and Ii, M. (2009). Analysis of binding site for the novel small-molecule TLR4 signal transduction inhibitor TAK-242 and its therapeutic effect on mouse sepsis model. Br J Pharmacol *157*, 1250-1262. 10.1111/j.1476-5381.2009.00297.x.
45. Kalaitzoglou, E., Lopes, E.B.P., Fu, Y., Herron, J.C., Flaming, J.M., Donovan, E.L., Hu, Y., Filiberti, A., Griffin, T.M., and Humphrey, M.B. (2019). TLR4 Promotes and DAP12 Limits Obesity-Induced Osteoarthritis in Aged Female Mice. JBMR Plus *3*, e10079. 10.1002/jbm4.10079.
46. Boyd, C.R., Orr, S.J., Spence, S., Burrows, J.F., Elliott, J., Carroll, H.P., Brennan, K., Gabhann, J.N., Coulter, W.A., Johnston, J.A., and Jefferies, C.A. (2009). Siglec-E Is Up-Regulated and Phosphorylated Following Lipopolysaccharide Stimulation in Order to Limit TLR-Driven Cytokine Production. The Journal of Immunology *183*, 7703-7709. 10.4049/jimmunol.0902780.
47. Ciesielska, A., Matyjek, M., and Kwiatkowska, K. (2021). TLR4 and CD14 trafficking and its influence on LPS-induced pro-inflammatory signaling. Cellular and Molecular Life Sciences *78*, 1233-1261. 10.1007/s00018-020-03656-y.
48. Klaus, C., Liao, H., Allendorf, D.H., Brown, G.C., and Neumann, H. (2021). Sialylation acts as a checkpoint for innate immune responses in the central nervous system. Glia *69*, 1619-1636. 10.1002/glia.23945.
49. Holehouse, A.S., and Kragelund, B.B. (2024). The molecular basis for cellular function of intrinsically disordered protein regions. Nature Reviews Molecular Cell Biology *25*, 187-211. 10.1038/s41580-023-00673-0.
50. Silva, Z., Rabaca, J.A., Luz, V., Lourenco, R.A., Salio, M., Oliveira, A.C., Bule, P., Springer, S., and Videira, P.A. (2024). New insights into the immunomodulatory potential of sialic acid on monocyte-derived dendritic cells. Cancer Immunol Immunother *74*, 9. 10.1007/s00262-024-03863-7.
51. Bull, C., Collado-Camps, E., Kers-Rebel, E.D., Heise, T., Sondergaard, J.N., den Brok, M.H., Schulte, B.M., Boltje, T.J., and Adema, G.J. (2017). Metabolic sialic acid blockade lowers the activation threshold of moDCs for TLR stimulation. Immunol Cell Biol *95*, 408-415. 10.1038/icb.2016.105.

52. Miyagi, T., and Yamaguchi, K. (2012). Mammalian sialidases: Physiological and pathological roles in cellular functions. Glycobiology *22*, 880-896. 10.1093/glycob/cws057.
53. Aljohani, M.A., Sasaki, H., and Sun, X.L. (2024). Cellular translocation and secretion of sialidases. J Biol Chem *300*, 107671. 10.1016/j.jbc.2024.107671.
54. Sundararaj, K., Rodgers, J., Angel, P., Wolf, B., and Nowling, T.K. (2021). The role of neuraminidase in TLR4-MAPK signalling and the release of cytokines by lupus serum-stimulated mesangial cells. Immunology *162*, 418-433. 10.1111/imm.13294.
55. Amith, S.R., Jayanth, P., Franchuk, S., Finlay, T., Seyrantepe, V., Beyaert, R., Pshezhetsky, A.V., and Szewczuk, M.R. (2010). Neu1 desialylation of sialyl alpha-2,3-linked beta-galactosyl residues of TOLL-like receptor 4 is essential for receptor activation and cellular signaling. Cell Signal *22*, 314-324. 10.1016/j.cellsig.2009.09.038.
56. Wang, Y., Khan, A., Antonopoulos, A., Bouché, L., Buckley, C.D., Filer, A., Raza, K., Li, K.-P., Tolusso, B., Gremese, E., et al. (2021). Loss of α2-6 sialylation promotes the transformation of synovial fibroblasts into a pro-inflammatory phenotype in arthritis. Nature Communications *12*. 10.1038/s41467-021-22365-z.
57. R Development Core Team (2023). A Language and Environment for Statistical Computing (R Foundation for Statistical Computing, Vienna, Austria).
58. R Development Core Team (2023). A Language and Environment for Statistical Computing. R Foundation for Statistical Computing, Vienna, Austria. https://www.R-project.org/.
59. Wickham, H., Hester, J., Bryan, J. (2024). readr: Read Rectangular Text Data. R package version 2.1.5. https://CRAN.R-project.org/package=readr.
60. Wickham, H., Averick, M., Bryan, J., Chang, W., McGowan, L.D.A., François, R., Grolemund, G., Hayes, A., Henry, L., Hester, J., et al. (2019). Welcome to the {tidyverse}. Journal of Open Source Software *4*, 1686. 10.21105/joss.01686.
61. Csárdi, G., . Nepusz, T,. Traag, V,. Horvát, Sz,. Zanini, F,. Noom, D,. Müller, K. (2025). igraph: Network Analysis and Visualization in R. doi.org/10.5281/zenodo.7682609.
62. Pedersen L. T (2024). ggraph: An Implementation of Grammar of Graphics for Graphs and Networks. R package version 2.2.1. https://CRAN.R-project.org/package=ggraph.
63. Wickham, H. (2016). ggplot2: Elegant Graphics for Data Analysis. Springer-Verlag New York.
64. Wickham, H., . Pedersen, T,. Seidel, D. (2023). _scales: Scale Functions for Visualization_. R package version 1.3.0, <https://CRAN.R-project.org/package=scales>.